A Journal of the Gesellschaft Deutscher Chemiker

Angewandte International Edition Chemie

GDCh

www.angewandte.org

Accepted Article

Title: Nanoisozymes: Crystal Facet-Dependent Enzyme Mimetic Activity of V2O5 Nanomaterials

Authors: Sourav Ghosh, Punarbasu Roy, Naiwrit Karmodak, Eluvathingal D. Jemmis, and Govindasamy Mugesh

To be cited as: *Angew. Chem. Int. Ed.* 10.1002/anie.201800681
Angew. Chem. 10.1002/ange.201800681

Link to VoR: http://dx.doi.org/10.1002/anie.201800681
http://dx.doi.org/10.1002/ange.201800681

WILEY-VCH

10.1002/anie.201800681

WILEY-VCH

Nanoisozymes: Crystal Facet-Dependent Enzyme Mimetic Activity of V_2O_5 Nanomaterials

*Sourav Ghosh, Punarbasu Roy, Naiwrit Karmodak, Eluvathingal D. Jemmis, and Govindasamy Mugesh**

Abstract: *Nanomaterials with enzyme-like activity (nanozymes) attract significant interest owing to their applications in biomedical research. Particularly, redox nanozymes that exhibit glutathione peroxidase (GPx)-like activity play important roles in cellular signalling by controlling the hydrogen peroxide (H_2O_2) level. Herein we report, for the first time, that the redox properties and GPx-like activity of V_2O_5 nanozyme depends not only on the size and morphology, but also on the crystal facets exposed on the surface within the same crystal system of the nanomaterials. These results suggest that the surface of the nanomaterials can be engineered to fine-tune their redox properties to act as "nanoisozymes" for specific biological applications.*

Hydrogen peroxide (H_2O_2) plays crucial roles in redox biology and cell signalling.[1] Cellular redox dynamics is regulated by feedback pathways that maintain the level of H_2O_2 below the toxic threshold. However, excessive amounts of H_2O_2 induce oxidative stress, resulting in damage to biomolecules such as DNA, proteins, and lipids.[2] In the long term, these damages lead to various disorders, such as neurodegeneration, HIV activation, cardiovascular diseases, cancer, and aging etc.[3] The antioxidant enzyme glutathione peroxidase (GPx) plays key roles in maintaining the redox homeostasis and protect the cells from oxidative damage.[4] A significant variation in the concentration of H_2O_2 required to initiate a particular biological response has been observed for different cell types. Therefore, multiple forms of GPx enzymes (isozymes) are known to control the intracellular as well as extracellular H_2O_2 levels using glutathione (GSH) as cofactor. Recent studies reveal that the peroxide-reducing ability of GPx4 isozyme prevents the iron-mediated ferroptosis, a novel form of non-apoptotic cell death.[5] At lower concentrations, H_2O_2 oxidizes cysteine residues on proteins to the corresponding sulfenic acids and initiates redox biology (Figure 1).[6] When the concentration of H_2O_2 is very high, the cysteine residues undergo irreversible oxidation to produce protein sulfinic and sulfonic acid species, which are biomarkers of oxidative stress. Further, the cysteine-containing peroxiredoxins (Prx), which are known to fine-tune the H_2O_2 levels, are inactivated by high levels of H_2O_2 as the thiol group in these proteins undergo overoxidation to sulfinic acid.[6c] In addition, elevated level of H_2O_2 leads to the formation of hydroxyl radicals (OH•), which together with other reactive oxygen species (ROS) such as peroxynitrite ($ONOO^-$) and hypochlorous acid (HOCl) damage biomolecules (Figure 1).[6]

[a] S. Ghosh, P. Roy, N. Karmodak, Prof. Dr. E. D. Jemmis, Prof. Dr. G. Mugesh
Department of Inorganic and Physical Chemistry
Indian Institute of Science, Bangalore-560012
E-mail: mugesh@iisc.ac.in

Supporting information of this article can be found under: https://doi.org/10.1002/anie.2018xxxx.

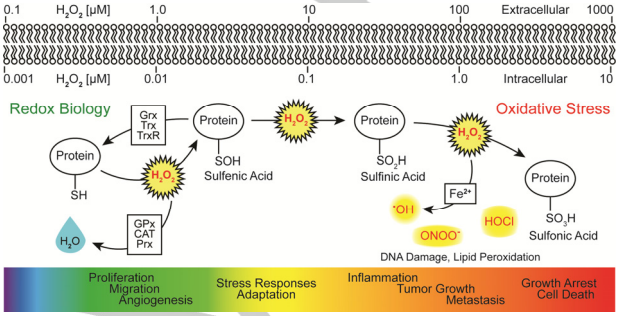

Figure 1. Estimated ranges of H_2O_2 concentration in oxidative stress with regard to cellular responses. Modified from Ref. [6] (Grx: glutaredoxin, Trx: thioredoxin, TrxR: thioredoxin reductase, Prx: peroxiredoxin).

Nanomaterials that mimic the function of redox enzymes have attracted significant interest.[7] Recently, we reported that V_2O_5 nanowires can protect cells from oxidative damage by exhibiting GPx-like activity in the presence of GSH.[8] This study revealed that the potentially toxic V_2O_5 can be turned into cytoprotective antioxidant by reducing the size of the material. It has been shown that bulk V_2O_5 or vanadium (V) complexes are highly toxic to the cells and modulation of the redox property of vanadium in the nano-form is crucial for its protective role. Previous studies showed that the catalytic performance of a nanomaterial, in general, can be altered by controlling the shape, size and surface coating.[9] The surface reactivity and redox behaviour depend greatly on the atomic arrangement of surface atoms and the number of dangling bonds on crystal facets.[10] However, the identification of enzyme-like active sites on nano-V_2O_5 has been difficult and it is unclear whether the GPx activity of this material depends on its size, shape and/or crystal facets. As maintenance of a desired redox activity is a challenging task, a detailed atomic-level understanding of nanozyme surfaces is crucial to design materials suitable for biomedical applications. In this paper, we report on the synthesis of orthorhombic V_2O_5 nanocrystals in different morphologies and show for the first time that alteration in the crystal facets within the same crystal system produces nanoisozymes capable of fine-tuning the desired redox activity. We also describe the nature of catalytically active species involved in the surface reactions using *in-situ* Raman spectroscopy.

For this study, we synthesized V_2O_5 nanocrystals in four different morphologies – nanowires (VN_W), nanosheets (VS_h), nanoflowers (VN_f) and nanospheres (VS_p). The scanning electron microscopy (SEM) and transmission electron microscopy (TEM) images confirmed the formation of four distinguishable morphologies of V_2O_5 nanocrystals (Figure 2a-d and Figure S1). The energy dispersive spectroscopy (EDS) and X-ray mapping confirmed the presence and distribution of vanadium (V) and oxygen (O) in all four materials (Figures S2

and S3). The crystalline nature of the nanomaterials was confirmed by powder X-ray diffractometer (XRD) (Figure S4) and the diffraction peaks were indexed to standard V_2O_5 orthorhombic phase (JCPDS = 41-1426, space group *Pmmn*).[11] To gain insight into the nature of bonding between the metal and oxygen atoms in the orthorhombic V_2O_5 crystals, FT-IR and FT-Raman spectra were recorded (Figure S5 and S6, Table S1 and S2). In the Raman spectra, the peak at 993 cm^{-1} corresponds to the terminal (V=O) resulting from unshared oxygen atom of the V_2O_5 crystal. The binding energies (BE) and full width at half maxima (FWHM) for the $V2p_{3/2}$ and $V2p_{1/2}$ peaks determined by X-ray photoelectron spectroscopy (XPS) analysis as well as the difference in the BE between O1s and $V2p_{3/2}$ orbitals (~12.7eV) confirm that vanadium exists in +5 oxidation state in all four morphologies (Figure S7, Table S3).[12]

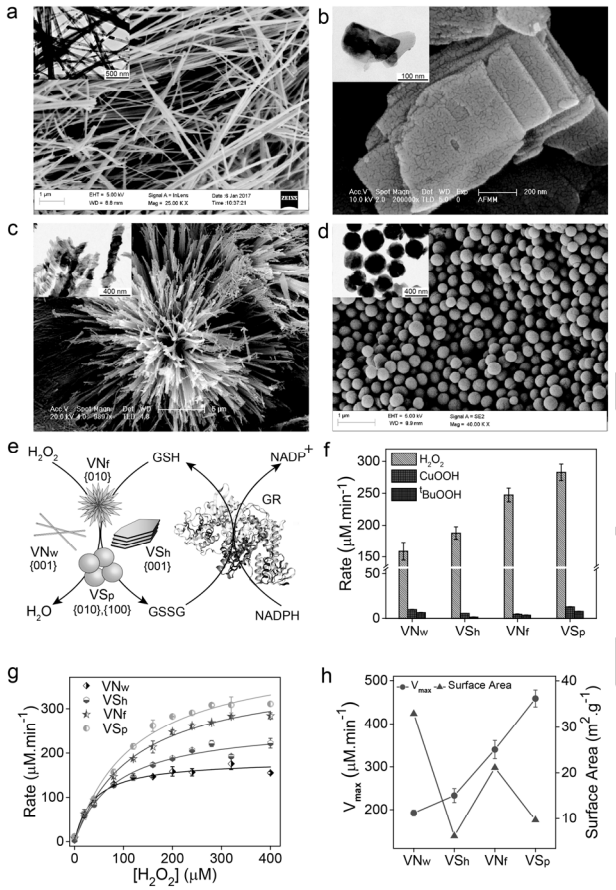

Figure 2. a-d) SEM and TEM (inset) images of VN_w, VS_h, VN_f and VS_p, respectively. e) Reduction of H_2O_2 by GSH in the presence of nanomaterials, glutathione reductase (GR) and NADPH. f) A comparison of the GPx-like reactivity in the presence of three different peroxides, H_2O_2, tert-butyl hydroperoxide (t-BuOOH) and cumene hydroperoxide (CuOOH). Assay conditions: nanozymes (20 ng.μL^{-1}), NADPH (0.2 mM), GSH (2 mM), GR (~1.7 units) peroxide (0.2 mM), in phosphate buffer (100 mM, pH 7.4) at 25ºC. g) Michaelis-Menten plot with varying concentration of H_2O_2 (0-400 μM) for all four nanozymes. h) Trend in V_{max} and surface area among the four nanozymes.

The reduction of H_2O_2 by the nanomaterials was monitored spectrophotometrically in the presence of GSH using glutathione reductase (GR) coupled assay.[8,7i] The rates of the reactions were determined by following the decrease in the absorbance of NADPH at 340 nm (Figure 2e). As shown in Figure 2f, all four materials were found to be highly efficient in catalysing the reduction of H_2O_2. A comparison of the activities of the nanomaterials with three different peroxides, H_2O_2, t-BuOOH and CuOOH, indicates that these materials are very selective to H_2O_2 as substrate. Interestingly, the nanosphere (VS_p) exhibited the highest activity in the series and the rate of reduction of H_2O_2 by VS_p was found to be almost two times higher than that of the nanowires (VN_w), indicating that the nanozyme activity of V_2O_5 is morphology dependent. Similar activities were observed when H_2O_2 was generated *in situ* using a glucose-glucose oxidase enzyme system (Figure S9).

To understand the substrate binding at the surface of the four nanomaterials, we studied the effect of H_2O_2 and GSH on the reaction rates and determined the kinetic parameters such as Michaelis constant (K_M), maximum velocity (V_{max}) using various concentrations of H_2O_2 (0-400 μM) and GSH (0-6 mM) under steady-state conditions. While a typical enzymatic Michaelis-Menten kinetics was observed for both the substrates (Figure 2g and Figure S10), the kinetic parameters obtained from the corresponding Lineweaver-Burk plots (Figure S11, S12 and Table S4) indicate that there are significant differences in the substrate binding. For H_2O_2, the K_M (μM) and V_{max} (μM.min^{-1}) values obtained for VN_w, (44.4 ± 1.7 and 192.3 ± 6.6), VS_h, (57.3 ± 3.8 and 233.1 ± 16.3), VN_f (92.5 ± 3.4 and 340.1 ± 21.3), and VS_p (143.7 ± 2.3 and 458.7 ± 19.6), respectively, indicate that the surface of the nanowires (VN_w) is saturated at lower concentration of H_2O_2, whereas a relatively higher concentrations of H_2O_2 are required for the saturation of the surface on nanosheets (VS_h). On the other hand, much higher concentrations of H_2O_2 are required for the saturation of surfaces on nanoflowers (VN_f) and nanospheres (VS_p).[7h] Interestingly, the K_M and V_{max} values mentioned above for different morphology do not correlate with their surface area (Figure 2h). The surface area and pore diameter determined by the Brunauer-Emmett-Teller (BET) method (Figure S13) indicate that VS_p with a relatively smaller surface area (9.7 $m^2.g^{-1}$) exhibits much higher activity as compared to VN_w with a larger surface area (32.9 $m^2.g^{-1}$).

The nanomaterials are capable of mediating multiple cycles of H_2O_2 reduction without loss of catalytic activity (Figure S14). The SEM and TEM experiments on nanomaterials isolated from the reaction mixture after the catalysis indicate that the materials are highly stable with no alterations in their morphology or surface (Figure S15). The activities obtained for the nanomaterials kept as dispersion in water for six months were identical to that of the freshly synthesized materials (Figure S16b). Further, the supernatant obtained after centrifugation of dispersed nanozymes at 6000 rpm for 20 min did not show any noticeable activity (Figure S16a), indicating that the intact surfaces and not leached metal ions are responsible for the observed activity.

The initial rates observed for various control reactions indicate that the nanozymes efficiently reduce H_2O_2 only in the presence of GSH and GR. (Figures 3a and S17). To understand the intermediates involved in the catalytic cycle, several *in-situ* FT-Raman spectra were recorded in the presence of VS_p (Figure 3b). The FT-Raman spectrum of pure VS_p showed a peak at 993 cm^{-1} for V-oxo (V=O) bond, which was not changed upon treatment with GSH, NADPH, and/or GR, suggesting that the V-oxo bond in the material is unaltered in the reducing conditions. This is in agreement with our earlier report that the vanadium(V)

center in V_2O_5 nanowires is not reduced by GSH.[8] In contrast, a significant decrease in the intensity of V=O peak was observed when H_2O_2 was added to the reaction mixture. This led to a rapid generation of a new peak at 1150 cm^{-1}, which can be assigned to the overtone peak for V-peroxido species.[13] These observations indicate that the reaction of V=O species with H_2O_2 is the first step of the catalytic cycle. Interestingly, a complete conversion of the V=O species to the V-peroxido intermediate was observed within 300 sec (Figure 3b). FT-Raman spectroscopic experiments with a sequential addition of H_2O_2 and GSH indicate that the V-peroxido species is the predominant intermediate in the catalytic cycle (Figure 3c and S19), which is further confirmed by time-dependent FT-IR of VN_w in the presence of H_2O_2 (Figure S20). A comparison of the reactivity of the V=O bond with H_2O_2 using the four different morphologies indicates that the formation of V-peroxido intermediate is most favoured on the surface of VS_p and rate of its formation follows the order VS_p > VN_f > VS_h > VN_w (Figure 3d-g and S18), which correlates well with their GPx-like activity.

The remarkable change in the reactivity of V=O bond and the overall catalytic activity indicate that the crystallographic orientation of the atoms on the surface or exposed facets on the surface play crucial roles. To understand the atomic arrangements of the exposed facets, we recorded high resolution TEM (HRTEM) and analysed the HRTEM images and their corresponding Fast-Fourier-Transform (FFT) patterns and obtained the direction of nanocrystal growth (zone axis) (Figure 4a-e and S21). The inter-planer distances and the angles between the planes observed in the HRTEM images were found to be in accordance with the crystal structure of V_2O_5 (JCPDS = 41-1426). It is observed that VN_w consists only of {001} facet, whereas the VS_h nanocrystals consist of both {001} and {010} facets, although the {010} is found to be a minor one. However, the {010} becomes the major exposed facet in VN_f, which also consists of a minor {001} facet. Interestingly, two major facets {100} and {010} are identified in VS_p along with two additional facets {-111}, {1-40}, which make the nanospheres different from the other three morphologies. The HRTEM images recorded after the reactions indicate that the exposed facets present on the surfaces of four different morphologies were unaffected by the catalysis (Figures 6b and S22).

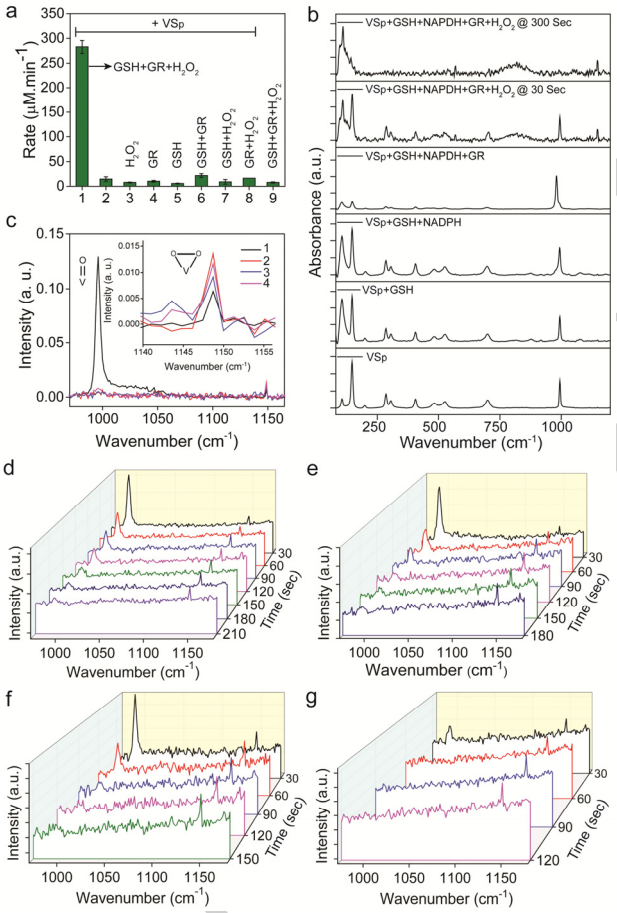

Figure 3. a) Reaction rates at different assay conditions for VS_p. b) Monitoring the formation of V-peroxido intermediate by *in-situ* Raman spectroscopy during GPx-like catlytic cycle of VS_p. c) Monitoring changes in the intensity of V=O and V-peroxido peaks by *in-situ* Raman spectroscopy on the surface of VS_p: 1. VS_p + H_2O_2 after 10 sec, 2. VS_p + H_2O_2 after 300 sec, 3. VS_p + H_2O_2 + GSH, 4. VS_p + H_2O_2 + GSH + H_2O_2. d-g) Time-dependent *in-situ* FT-Raman spectroscopy recorded after the addition of H_2O_2 (5 mM) to VN_w, VS_h, VN_f and VS_p, respectively.

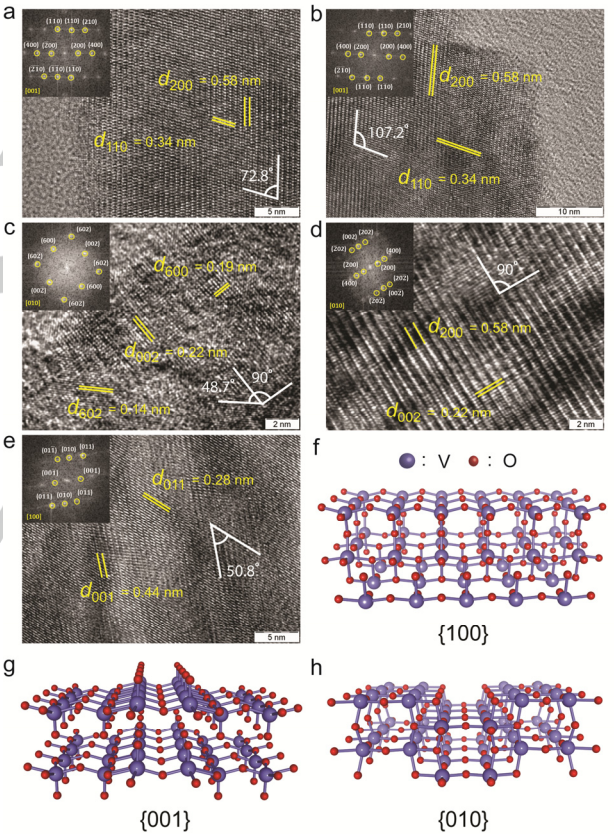

Figure 4. HRTEM and Fast-Fourier-Transform (inset) pattern of a) VN_w, b) VS_h, c) VN_f, d and e) VS_p. f-h) Atomic arrangements of {100}, {001}, and {010} crystal facets respectively.

As the reaction of nanomaterials with H_2O_2 is a crucial step in the catalytic cycle, we carried out quantum chemical calculations using density functional theory (DFT) to understand the reactivity of the exposed facets with H_2O_2. The reactivity was compared by calculating the energy of H_2O_2 adsorption (ΔE_1) and formation of V-peroxido intermediate (ΔE_2) on the surfaces.[13] The total energy change (ΔE_{tot}) for the reaction of H_2O_2 on the surface was obtained as sum of ΔE_1 and ΔE_2.

Among several possibilities, the most favoured orientations of H_2O_2 on these surfaces are shown along with ΔE_1, ΔE_2 and ΔE_{tot} in Figure 5b-f. The other possibilities are provided in the Supplementary Information (Figure S28, S29 and S30). One of the oxygen atoms in H_2O_2 was found to interact with the surface vanadium atoms, whereas the hydrogen atoms interacted with the oxygen atoms of V=O and V-O-V groups. This led to an elongation of the vanadium-oxygen bond lengths as well as the O-H bond in H_2O_2 as shown in Figure 5. The formation of V-peroxido species was not observed on {001} facet, which had the lowest adsorption energy. In {001} facet, the vanadium is coordinatively saturated, which is similar to that of weakly bound layers of bulk V_2O_5 (Figure 4g). The {100} and {010} facets had higher ΔE_1 values and the formation of V-peroxido intermediate was found to be exothermic in nature with {010} facet having the highest ΔE_{tot} value. In addition to the formation of V-peroxido intermediate on the surface, the hydrogen atoms of H_2O_2 formed V-OH bonds, which can abstract a proton from second molecule of H_2O_2 to eliminate a water molecule. The greater reactivity of {100} and {010} facets is due to the unsaturated coordination around the surface vanadium atoms. In these two facets, the vanadium atoms present on the surface are connected to four oxygen atoms (Figure 4f,h and S27). The difference in the reactivity of the facets with H_2O_2 can also be ascribed to the variation in the surface formation energy (E_{FS}), which is calculated as $E_{FS} = (E_{surface}-E_{bulk})/A_{surface}$ ($E_{surface}$ and E_{bulk} correspond to the optimized energy of the surface and bulk V_2O_5 crystal, respectively and $A_{surface}$ is the area of V_2O_5 nano-surfaces). For {100} an {010}, the E_{FS} values are 0.05 eV/Å^2 and 0.08 eV/Å^2 higher than that of {001}. These observations suggest that the {010} facet is the most reactive surface, whereas the {001} facet is the least active one, which is in agreement with the catalytic activity of VN_w, VS_h, VN_f and VS_p.

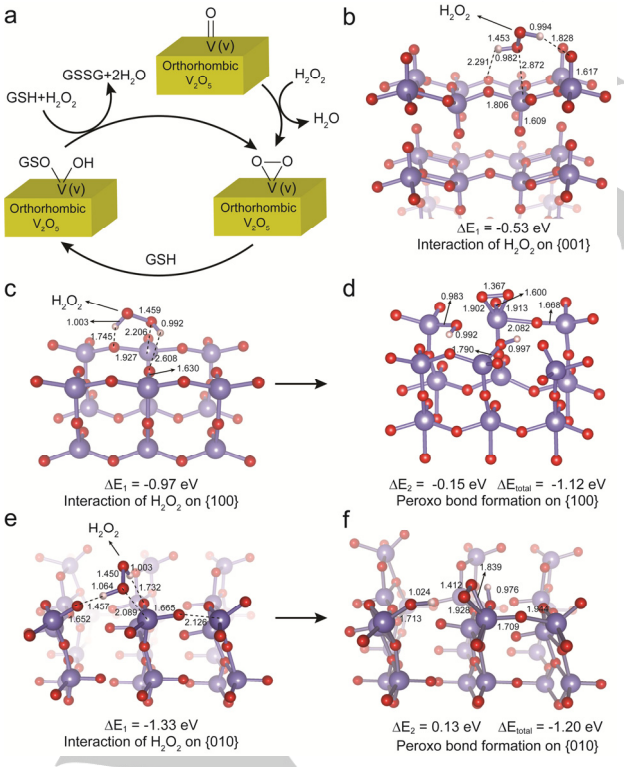

Figure 5. a) Schematic representation of the reaction of H_2O_2 and GSH on the surface of orthorhombic V_2O_5 crystal. b, c and e) Most favoured orientation for interaction of H_2O_2 with {001}, {100} and {010} crystal facets respectively. d and f) V-peroxido intermediate on {100} and {010}, respectively.

As an optimum level of H_2O_2 is required for the desired redox biology and cell signalling and different isoforms of GPx enzymes control the level of H_2O_2 in a compartment-specific manner, it was thought worthwhile to investigate the GPx activity of the nanozymes at different ratios of GSH/H_2O_2. It should be noted that GSH is required for the cleavage as well as regeneration of the V-peroxido species as shown in Figure 5a. The initial reaction rates were measured by increasing the concentration of H_2O_2 (Figure 6a). When the concentration of H_2O_2 was 100- or 50-fold lower than that of GSH, all the materials exhibited similar GPx-like activity. When the concentration of H_2O_2 was increased, a significant difference in the catalytic activity was observed. Interestingly, the activity of nanospheres (VS_p) increased rapidly with an increase in the concentration of H_2O_2 and at GSH/H_2O_2 ratio of 5, the activity was found to be remarkably higher than that of nanowires (VN_w). In fact, the GPx activity of VN_w was almost unaltered over a large range of H_2O_2 concentrations. The response of VN_f was found to be similar to that of VS_p, indicating that these two materials can exhibit high GPx activity at higher peroxide concentrations and depleted GSH levels, i.e. oxidative stress conditions. It should be noted that GSH has a significant role in the maintenance of cellular redox state through changes in thiol/disulphide equilibrium potential.[14] The solid-state electrochemical responses (cyclic voltammograms) of different morphologies indicated significant shifts in their oxidation-reduction potentials (Figure S26, Table S5).

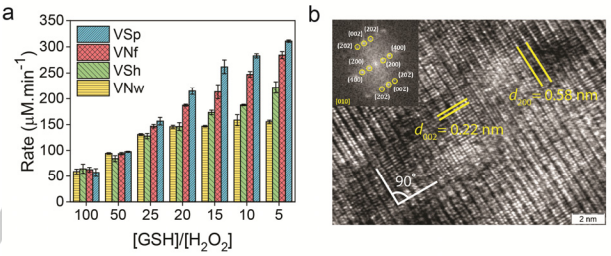

Figure 6. a) GPx activity of different nanozymes (20 ng.μL^{-1}) at various [GSH]/[H_2O_2] ratios in phosphate buffer, 0.1 mM, pH 7.4 at 25°C. The concentrations of GSH, GR and NADPH were fixed at 2.0 mM, 1.7 Units and 0.2 mM, respectively. b) HRTEM and corresponding FFT (inset) of VS_p after catalysis.

These differences suggest that the extent of polarization of the surface and migration of electrons between the atomic layers depend on the crystal facet and morphology.[15] Understanding of the redox potentials of various morphologies is important from the biological perspective as a 40 mV change in the reduction potential of GSH in healthy cells causes growth arrest and a further 50-70 mV change can lead to apoptotic or necrotic cell death.[14a]

In conclusion, we report the synthesis and glutathione peroxidase-like enzyme mimetic activity of orthorhombic V_2O_5 nanozymes in four different morphologies, nanowires (VN_w), nanosheets (VS_h), nanoflowers (VN_f) and nanospheres (VS_p) and show that the activity does not correlate with their surface area. We demonstrate for the first time that the surface exposed crystal facets within the same crystal system can alter the H_2O_2 reducing ability of V_2O_5 nanozymes. The activity depends on the

relative concentrations of H_2O_2 and glutathione (GSH) and at higher H_2O_2 concentrations, the nanospheres exhibit remarkably higher activity as compared to that of nanowires, indicating that the crystal facets play crucial roles in the catalytic activity. The variations in the GPx-like activity originate from the difference in the rate of formation of a V-peroxido species on the surface. The results described in this paper on the modulation of redox reactions by altering the size, shape and crystal facets may open up opportunities not only for the design and synthesis of nanomaterials with enzyme-like activity, but also for the development of nanomaterial-based isozymes (nanoisozymes), which essentially catalyse the same chemical reactions, but exhibit a compartment-specific activity in biological systems.

Acknowledgements

This study was supported by the Science and Engineering Research Board (EMR/IISc-01/2016) and DST Nanomission (SR/NM/NS-1380/2014), New Delhi. G.M. and EDJ acknowledge the SERB/DST for the award of J. C. Bose National Fellowship. S. G. and P. R. thank the Indian Institute Science, Bangalore, and N.K. thanks the CSIR, New Delhi for the fellowships. The authors thank Dr. A. A. Vernekar, Prof. N. Munichandraiah, Dr. R. Viswanatha, Dr. B. Kishore and Mr. S. Prasad for their support and help with some of the experiments. We also thank the MNCF Facility, CeNSE, IISc for the spectroscopic and microscopic facilities.

Conflict of interest

The authors declare no conflict of interest.

Keywords: antioxidants • crystal facet • glutathione peroxidase • nanozymes • oxidative stress

[1] a) V. Adler, Z. Yin, K. D. Tew, Z. Ronai, *Oncogene* **1999**, *18*, 6104–6111; b) B. D'Autréaux, M. B. Toledano, *Nat. Rev. Mol. Cell Biol.* **2007**, *8*, 813–824; c) M. Schieber, N. S. Chandel, *Curr. Biol.* **2014**, *24*, R453–R462; d) H. Sies, *Redox Biol.* **2015**, *4*, 180–183; e) C. Lennicke, J. Rahn, R. Lichtenfels, L. A. Wessjohann, B. Seliger, *Cell Commun. Signal.* **2015**, *13*, 1–19; f) R. Mittler, *Trends Plant Sci.* **2017**, *22*, 11–19.

[2] a) K. J. Davies, *J Biol Chem.* **1987**, *262*, 9895-9901; b) A. Terman, U. T. Brunk, *Antioxid. & Redox Signal.* **2006**, *8*, 197-204; c) I. Dalle-Donne, G. Aldini, M. Carini, R. Colombo, R. Rossi, A. Milzani, *J. Cell Mol. Med.* **2006**, *10*, 389-406; d) E. Ju, K. Dong, Z. Chen, Z. Liu, C. Liu, Y. Huang, Z. Wang, F. Pu, J. Ren, X. Qu, *Angew. Chem. Int. Ed.* **2016**, *55*, 11467–11471.

[3] a) O. I. Aruoma, *Jaocs* **1998**, *75*, 199–212; b) T. Finkel, N. J. Holbrook, *Nature* **2000**, *408*, 239–247; c) K. J. Barnham, C. L. Masters, A. I. Bush, *Nat. Rev. Drug Discov.* **2004**, *3*, 205–214.

[4] a) J. R. Arthur, *Cell. Mol. Life Sci.* **2001**, *57*, 1825–1835; b) E. V. Kalinina, N. N. Chernov, M. D. Novichkova, *Biochem.* **2014**, *79*, 1562–1583.

[5] a) S. J. Dixon, K. M. Lemberg, M. R. Lamprecht, R. Skouta, E. M. Zaitsev, C. E. Gleason, D. N. Patel, A. J. Bauer, A. M. Cantley, W. S. Yang, B. Morrison, B. R. Stockwell, *Cell* **2012**, *149*, 1060–1072; b) W. S. Yang, R. Sriramaratnam, M. E. Welsch, K. Shimada, R. Skouta, V. S. Viswanathan, J. H. Cheah, P. A. Clemons, A. F. Shamji, C. B. Clish, L. M. Brown, A. W. Girotti, V. W. Cornish, S. L. Schreiber, B. R. Stockwell, *Cell* **2014**, *156*, 317–331.

[6] a) H. Sies, *Redox Biol.* **2017**, *11*, 613–619; b) H. S. Marinho, C. Real, L. Cyrne, H. Soares, F. Antunes, *Redox Biol.* **2014**, *2*, 535–562; c) T. Rabilloud, M. Heller, F. Gasnier, S. Luche, C. Rey, R. Aebersold, M. Benahmed, P. Louisot, J. Lunardi, *J. Biol. Chem.* **2002**, *277*, 19396–19401.

[7] a) R. André, F. Natálio, M. Humanes, J. Leppin, K. Heinze, R. Wever, H. C. Schröder, W. E. G. Müller, W. Tremel, *Adv. Funct. Mater.* **2011**, *21*, 501–509; b) Z. Chen, J. J. Yin, Y. T. Zhou, Y. Zhang, L. Song, M. Song, S. Hu, N. Gu, *ACS Nano* **2012**, *6*, 4001–4012; c) H. Wei, E. Wang, *Chem. Soc. Rev.* **2013**, *42*, 6060-6093; d) J. Dong, L. Song, J. J. Yin, W. He, Y. Wu, N. Gu, Y. Zhang, *ACS Appl. Mater. Interfaces* **2014**, *6*, 1959–1970; e) Y. Lin, J. Ren, X. Qu, *Acc. Chem. Res.* **2014**, *47*, 1097–1105; f) R. Ragg, M. N. Tahir, W. Tremel, *Eur. J. Inorg. Chem.* **2016**, *2016*, 1906–1915; g) Y. Huang, Z. Liu, C. Liu, E. Ju, Y. Zhang, J. Ren, X. Qu, *Angew. Chem. Int. Ed.* **2016**, *55*, 6646–6650; h) A. A. Vernekar, T. Das, G. Mugesh, *Angew. Chem. Int. Ed.* **2016**, *55*, 1412–1416; i) N. Singh, M. A. Savanur, S. Srivastava, P. D'Silva, G. Mugesh, *Angew. Chem. Int. Ed.* **2017**, *56*, 14267–14271; j) X. Wang, Y. Hu, H. Wei, *Inorg. Chem. Front.* **2016**, *3*, 41-60; k) H. Cheng, Y. Liu, Y. Hu, Y. Ding, S. Lin, W. Cao, Q. Wang, J. Wu, F. Muhammad, X. Zhao, D. Zhao, Z. Li, H. Xing, H. Wei, *Anal. Chem.* **2017**, *89*, 11552-11559; l) Y. Hu, H. Cheng, X. Zhao, J. Wu, F. Muhammad, S. Lin, J. He, L. Zhou, C. Zhang, Y. Deng, P. Wang, Z. Zhou, S. Nie, H. Wei. *ACS Nano* **2017**, *11*, 5558–5566.

[8] A. A. Vernekar, D. Sinha, S. Srivastava, P. U. Paramasivam, P. D'Silva, G. Mugesh, *Nat. Commun.* **2014**, *5*, 6301.

[9] a) L. Hu, Q. Peng, Y. Li, *J. Am. Chem. Soc.* **2008**, *130*, 16136–16137; b) A. X. Yin, X. Q. Min, Y. W. Zhang, C. H. Yan, *J. Am. Chem. Soc.* **2011**, *133*, 3816–3819; c) J. Mu, L. Zhang, G. Zhao, Y. Wang, *Phys. Chem. Chem. Phys.* **2014**, *16*, 15709-15716; d) E. W. Zhao, H. Zheng, R. Zhou, H. E. Hagelin-Weaver, C. R. Bowers, *Angew. Chem. Int. Ed.* **2015**, *54*, 14270–14275; e) Z. Zhang, X. Zhang, B. Liu, J. Liu, *J. Am. Chem. Soc.* **2017**, *139*, 5412–5419; e) M. J. Manto, P. Xie, C. Wang, *ACS Catal.* **2017**, *7*, 1931–1938.

[10] a) J. E. Park, M. Son, M. Hong, G. Lee, H. C. Choi, *Angew. Chem. Int. Ed.* **2012**, *51*, 6383–6388; b) J. Jiang, K. Zhao, X. Xiao, L. Zhang, *J. Am. Chem. Soc.* **2012**, *134*, 4473–4476; c) C. Li, C. Koenigsmann, W. Ding, B. Rudshteyn, K. R. Yang, K. P. Regan, S. J. Konezny, V. S. Batista, G. W. Brudvig, C. A. Schmuttenmaer, J. H. Kim, *J. Am. Chem. Soc.* **2015**, *137*, 1520–1529; d) C. Ge, G. Fang, X. Shen, Y. Chong, W. G. Wamer, X. Gao, Z. Chai, C. Chen, J. J. Yin, *ACS Nano* **2016**, *10*, 10436–10445; e) C. S. Tan, P. L. Hsieh, L. J. Chen, M. H. Huang, *Angew. Chem. Int. Ed.* **2017**, *56*, 15339–15343; f) C. Yang, X. Yu, S. Heissler, P. Weidler, A. Nefedov, Y. Wang, C. Wöll, T. Kropp, J. Paier, J. Sauer, *Angew. Chem. Int. Ed.* **2017**, *56*, 16399–16404.

[11] F. Zhou, X. Zhao, C. Yuan, L. Li, *Cryst. Growth Des.* **2008**, *8*, 723–727.

[12] E. Hryha, E. Rutqvist, L. Nyborg, *Surf. Interface Anal.* **2012**, *44*, 1022–1025.

[13] J. E. Molinari, I. E. Wachs, *J. Am. Chem. Soc.* **2010**, *132*, 12559–12561.

[14] a) M. L. Circu, T. Y. Aw, *Free Radic. Res.* **2011**, *45*, 1245–1266; b) L. Flohé, *Biochim. Biophys. Acta,* **2013**, *1830*, 3139–3142; c) Y. Huang, F. Pu, J. Ren, X. Qu, *Chem. Eur. J.* **2017**, *23*, 9156-9161.

[15] M. Ek, Q. M. Ramasse, L. Arnarson, P. Georg Moses, S. Helveg, *Nat. Commun.* **2017**, *8*, 305.

10.1002/anie.201800681

WILEY-VCH

COMMUNICATION

The first experimental evidence for the crystal facet-dependent enzyme mimetic activity of V_2O_5 nanozymes is described. The activity of the four nanoforms of V_2O_5 namely wires, sheets, floweres and spheres exhibit different redox modulatory effect in the presence of H_2O_2.

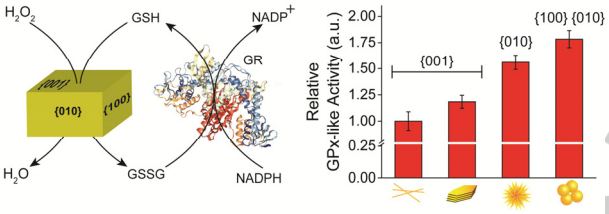

*Sourav Ghosh, Punarbasu Roy, Naiwrit Karmodak, Eluvathingal D. Jemmis, Govindasamy Mugesh**

Page No. – Page No.

Nanoisozymes: Crystal Facet-Dependent Enzyme Mimetic Activity of V_2O_5 Nanomaterials